

1 *Paper accepted in April 2010 for publication by the Canadian J. of Civil Engineering*

2  
3 **FLEXURAL BEHAVIOUR OF CONCRETE BEAMS STRENGTHENED WITH**  
4 **NEAR SURFACE MOUNTED FRP BARS**

5  
6  
7 **Shehab M. Soliman<sup>1</sup>, Ehab El-Salakawy<sup>2</sup>, and Brahim Benmokrane<sup>3</sup>**

8 <sup>3</sup>Corresponding Author

9  
10 

---

<sup>1</sup> Ph. D. Candidate, Department of Civil Engineering, University of Sherbrooke,  
11 Sherbrooke, Quebec, Canada J1K 2R1, Phone: (819) 821-8000 ext. 65178, Fax: (819) 821-  
12 7974, E-mail: Shehab.Soliman@USherbrooke.ca

13  
14 <sup>2</sup> Associate Professor and Canada Research Chair in Advanced Composite Materials and  
15 Monitoring of Civil Infrastructures, Department of Civil Engineering, University of  
16 Manitoba, Winnipeg, Manitoba, Canada, R3T 5V6, Tel: (204) 474-8319 Fax: (204) 474-  
17 7513 E-mail: [Ehab\\_Elsalakawy@Umanitoba.ca](mailto:Ehab_Elsalakawy@Umanitoba.ca)

18  
19 <sup>3</sup> NSERC Research Chair Professor in Innovative FRP Composite Materials for  
20 Infrastructures, Department of Civil Engineering, University of Sherbrooke, Sherbrooke,  
21 Quebec, Canada, J1K 2R1, Phone: (819) 821-7758, Fax: (819) 821-7974, E-mail:  
22 Brahim.Benmokrane@USherbrooke.ca

23

1

2 **ABSTRACT:** Fibre reinforced polymer (FRP) composite materials have been used as  
3 internal and external reinforcement for concrete structures. Flexural strengthening of  
4 concrete elements using near-surface mounted (NSM)-FRP materials is a promising  
5 technology. Although research on this topic has been started over the last 10 years, it has  
6 attracted worldwide attention. This research is designed to investigate the behaviour of  
7 reinforced concrete beams strengthened in flexure with NSM-FRP bars. A total of twenty  
8 reinforced concrete beams (3100-mm long  $\times$  200-mm wide  $\times$  300-mm deep) were  
9 constructed and tested till failure. Different parameters including internal steel  
10 reinforcement ratio, type of NSM-FRP bars, FRP bar diameter, bonded length and groove  
11 size were investigated in this research. Test results showed that the use of NSM-FRP bars  
12 is effective in increasing the flexural capacity of concrete beams. In addition, an  
13 incremental nonlinear displacement-controlled 3D finite element (FE) analysis was used  
14 to numerically simulate the behaviour of the test beams. A recently developed bond-slip  
15 relationship was adopted in the numerical simulations to characterize the behaviour of the  
16 FRP/epoxy and epoxy/concrete interfaces. Comparisons between the FE predictions and  
17 experimental results showed very good agreement in terms of the load-deflection and  
18 load-strain relationships, ultimate capacities, and modes of failure for the tested beams.

19

20 **Key words:** fibre reinforced polymer (FRP); near surface mounted (NSM); reinforced  
21 concrete beams; flexural strengthening; finite element analysis.

22

## 1 INTRODUCTION

2 Due to their superior characteristics and non-corrodible nature, fibre reinforced polymer  
3 (FRP) composite materials have been recently used as a replacement for steel  
4 reinforcement in concrete structures. In the last few years, near surface mounting (NSM)  
5 technique has received more attention as an alternative for externally-bonded (EB) FRP  
6 laminates in the flexural strengthening of concrete elements (Teng et al. 2006; Cruz and  
7 Barros 2006; Soliman et al. 2007; Nanni et al. 2004). Major innovative applications have  
8 been witnessed in this field to overcome the problems arising when EB-FRP composites  
9 are subjected to severe environmental conditions or mechanical damage (Hassan and  
10 Rizkalla 2004; Kotynia 2007; Soliman et al. 2008). In this strengthening technique,  
11 longitudinal grooves are first cut into the concrete cover of beams or slabs, then the  
12 reinforcing bars are inserted into these grooves and bonded with an appropriate binding  
13 agent; typically an epoxy paste or a cement grout. The first application of this technique  
14 was the implementation of steel bars into slots to strengthen a bridge deck slab in  
15 Lapland, Finland in 1940s (Asplund 1949).

16 Based on the results of several applications (El-Hacha and Rizkalla 2004), it has been  
17 concluded that the increase in the flexural capacity of strengthened beams applying NSM  
18 technique is greater than that using externally-bonded systems for the same axial stiffness  
19 of the FRP laminates. This is attributed to the fact that the NSM method delays the  
20 debonding of the FRP laminate, and thus increases the load carrying capacity and the  
21 FRP strength utilization ratio; the ratio of the strain in the FRP at failure to its ultimate  
22 strain.

1 Unlike the unstrengthened concrete beams, the failure of a FRP-strengthened beam is  
2 generally governed by separation of the concrete cover either at the end of the FRP  
3 laminates or between two intermediate cracks. These premature failures, caused by  
4 debonding, often limit the effectiveness of this strengthening technique and prevent these  
5 beams from attaining their ultimate flexural capacities (De Lorenzis and Teng 2007).  
6 However, these debonding failures are less likely to occur with NSM-FRP rods compared  
7 to those with EB-FRP sheets. To date, our knowledge of the various debonding  
8 phenomena and the associated mechanics of the bond between the NSM-FRP rods and  
9 concrete are somewhat limited. Further details on the advancements related to using  
10 NSM strengthening technique can be found in various state-of-the-art reports and review  
11 papers (De Lorenzis and Teng 2007).

12 As far as numerical modelling is concerned, few investigations were carried out to  
13 simulate the behaviour of beams strengthened with NSM-FRP systems (Hassan and  
14 Rizkalla 2004; Kange et al. 2005). Although no failure criterion has been introduced in  
15 the literature to simulate the debonding phenomena of NSM-FRP strips from the  
16 surrounding concrete layer, these numerical simulations predict with a reasonable  
17 accuracy the load–deflection profiles as claimed by their proponents. This may be due to  
18 the fact that these models simulated beams tested in particular experimental programs  
19 employing the experimentally-measured values of the debonding strain in the numerical  
20 models.

21 The limited number of the finite element simulations of NSM-FRP-strengthened concrete  
22 beams is due to the lack of knowledge on the interfacial behaviour between the FRP and  
23 concrete and the bond mechanisms involved. A failure criterion that defines the

1 termination of the analysis according to the strain limit in the FRP is still missing.  
2 Therefore, this paper introduces an attempt to present a 3D nonlinear finite element  
3 analysis for NSM-FRP-strengthened beams taking into account the interfacial behaviour  
4 between FRP bars and surrounding concrete. Accordingly, this research is one of the first  
5 attempts to consider the relative slip between the NSM bars and concrete beams in the  
6 numerical simulations.

7

## 8 **BACKGROUND**

9 During the last few years, an extensive research work to investigate, develop and  
10 implement sand-coated FRP reinforcing bars in new concrete structures has been going  
11 on at the University of Sherbrooke (El-Salakawy, et al. 2004; Benmokrane et al. 2005  
12 and 2006). However, the use of these FRP bars in strengthening of existing structures is  
13 still to be investigated. Therefore, the main objectives of the presented research project  
14 are: (1) to develop/utilize a NSM system composed of sand-coated FRP bars (Pultrall Inc.  
15 2006) and adhesives (Hilti Inc. 2006); both manufactured and produced in Canada; (2) to  
16 study the flexural behaviour of concrete beams strengthened with NSM-FRP bars, in  
17 terms of cracking, deflection, carrying capacity, and mode of failure, having different  
18 parameters; and (3) to construct an analytical model using non-linear finite element  
19 analysis (ADINA 2004) taking into consideration the interfacial behaviour between  
20 concrete and FRP bars.

21

22

23

# 1 **EXPERIMENTAL PROGRAM**

## 2 **Material Properties**

3 All tested specimens were constructed using a ready-mixed concrete with a targeted 28-  
4 day concrete compressive strength of 35 MPa. The actual concrete compressive and  
5 tensile strengths were determined based on standard cylinder tests at the same time of  
6 testing the specimens. The obtained concrete compressive and tensile strengths were 41  
7 and 3.3MPa, respectively.

8 Two types of sand-coated FRP bars, carbon and glass (Pultrall Inc. 2006) were used in  
9 this study. Two diameters were used for carbon FRP (No. 10, 9.5 mm and No. 13, 12.7  
10 mm), while only one diameter (No. 13, 12.7 mm) was used for glass FRP. Also,  
11 deformed steel bars No.10 (11.3 mm-diameter) and No.15 (15.9 mm-diameter) were used  
12 in reinforcing the concrete beams. The material propoerties of the used FRP and steel  
13 bars were obtained in the laboratory according to the appropriate standard (ACI  
14 Committee 440 2004) as listed in Table 1.

15 A high strength two-part epoxy based adhesive, type HIT RE 500 (Hilti Inc. 2005), was  
16 used in this study. This type of adhesive, which can be applied on wet or dry surfaces, is  
17 specially designed for fastening into solid base materials in a wide range of material  
18 temperatures (49°C down to -5°C). According to the manufacturet, the tensile strength  
19 and modulus of elasticity of the HIT RE 500 adhesive are 43.5 and 1493 MPa,  
20 respectively.

21

22

23

## 1 **NSM Strengthening Scheme**

2 Following the 28-day curing period, the test beams were placed upside down to be  
3 prepared for cutting the grooves. A special concrete saw, with a diamond blade, was used  
4 to make two cuts in the beam surface, then the concrete in between was chopped by  
5 means of a small power chisel. The grooves were cleaned with a steel brush followed by  
6 pressurized air. The epoxy was injected into the groove to cover about  $2/3$  of the groove  
7 depth. The bar was gently inserted into the groove over a plastic support outside the  
8 bonded length to maintain the thickness of the epoxy and to center the bar in the middle  
9 of the groove. The bar was gently pressed to displace the bonding agent. Additional  
10 adhesive was added to fill the groove and the surface of the epoxy was levelled.

11

## 12 **Test Specimens, Setup and Procedure**

13 A total of twenty reinforced concrete beams were constructed and tested to failure. The  
14 beams measured 3010-mm in length, 200-mm in width and 300-mm in depth. The beams  
15 are divided to three series; A, B and C, according to their tension steel reinforcement  
16 ratios. All beams were designed to fail in flexure by yielding of steel reinforcement. Two  
17 No.10 steel bars were used as compression reinforcement for all the tested beams.  
18 Typical smooth 8-mm diameter steel stirrups were used in all beams with a spacing of  
19 100 mm over the whole length of the beam to avoid shear failure. For each beam, only  
20 one NSM-FRP bar was used at the middle of a square groove. Except beams AC5, AC6  
21 and AC7, the square groove measured  $2d$ ; where  $d$  is the diameter of the used NSM-FRP  
22 bar. For beams AC5, AC6 and AC7, the square groove measured  $1.5d$ . Figure 1 shows  
23 the dimension and the reinforcement details for each series.

1

## 2 **Series A**

3 A total of twelve beams with a tension reinforcement ratio of 0.4% (2 No.10) were tested  
4 in series A. One unstrengthened beam, A0, was tested as a control specimen. Four beams,  
5 AC1 to AC4 were strengthened with 9.5-mm diameter NSM-CFRP bars having  $12d$ ,  $24d$ ,  
6  $48d$  and  $60d$  bonded lengths. Three beams, AC5, AC6 and AC7 were strengthened with  
7 one 9.5-mm diameter NSM-CFRP bar with  $24d$ ,  $48d$  and  $60d$  bonded lengths (square  
8 groove equals to  $1.5d$ ). Two beams, AC8 and AC9 were strengthened using 12.7-mm  
9 diameter NSM-CFRP bars with  $24d$  and  $48d$  bonded lengths, respectively. This  
10 represents an increase in the NSM-CFRP area of 79%. Beams AG10 and AG11 were  
11 similar to AC8 and AC9, respectively, but using 12.7-mm diameter GFRP bars. The  
12 objectives of this series were to investigate the effects of increasing the bonded length,  
13 decreasing the groove size, increasing the NSM-FRP area and the feasibility of using  
14 GFRP bars in strengthening. Table 3 summarizes the test matrix.

15

## 16 **Series B**

17 Only three beams with a tension reinforcement ratio of 0.8% (2 No.15) were tested in  
18 series B. One unstrengthened beam, B0, was tested as a control specimen and two beams  
19 were strengthened with 9.5-mm diameter NSM-CFRP bars. Beams BC1 and BC2 were  
20 strengthened with  $24d$  and  $48d$  bonded lengths, respectively. The objective of this series  
21 was to investigate the effects of increasing the amount of internal steel reinforcement to a  
22 moderate ratio (double the ratio of series A) on the behaviour of strengthened beams.

23

## 1 **Series C**

2 A total of five beams with a tension reinforcement ratio of 1.6% (4 No.15) were tested in  
3 series C. One unstrengthened beam, C0, was tested as a control specimen. While, the  
4 other four beams, AC1 to AC4, were strengthened with a 9.5-mm diameter CFRP bar.  
5 The bonded length of the NSM-CFRP bar at each end of beams CC1, CC2, CC3 and CC4  
6 was  $12d$ ,  $18d$ ,  $24d$  and  $48d$ , respectively. The objective of this series was to investigate  
7 the effects of increasing the amount of internal steel reinforcement to a relatively high  
8 ratio (double the ratio of series B) on the behaviour of strengthened beams.

9

## 10 **Test Set-Up and Instrumentation**

11 The beams were tested in four-point bending over a simply-supported clear span of 2.6 m  
12 as shown in Fig. 2. A 500-kN closed-loop MTS actuator was used to apply the load as  
13 shown in. The displacement-controlled rate of loading was 1.2 mm/min up to failure. A  
14 combination of electrical strain gauges and linear variable differential transducers  
15 (LVDTs) with different stroke lengths was used to monitor deflections, crack width, and  
16 NSM-FRP end-slip during testing.

17

## 18 **Test Results and Discussion**

### 19 **General behaviour**

20 Table 3 and Fig. 3 show the test results and the load-deflection relationships,  
21 respectively, for the tested beams. All beams failed by debonding in the form of concrete  
22 cover splitting at the level of steel reinforcement. The debonding process started at the

1 cut-off points of the NSM-FRP bar. However, the control beams failed by steel yielding  
2 followed by concrete crushing.

3 For the strengthened beams, the figure shows that the load-deflection relationship is a tri-  
4 linear. The first line is up to cracking where all the strengthened beams exhibited similar  
5 behaviour to the unstrengthened beam. This means that the NSM-FRP reinforcement had  
6 insignificant contribution to the increase of stiffness or strength before cracking. The  
7 second line is between cracking and yielding of the internal steel reinforcement. In this  
8 stage, the flexural stiffness of the strengthened specimens was significantly increased  
9 compared to the unstrengthened one. The NSM-FRP bar provided constraints to the  
10 opening of the cracks resulting in an increase of the moment of inertia of the cracked  
11 section. The third line is between yielding of internal steel and debonding of the NSM-  
12 FRP bar, which represent the enhancement in both strength and stiffness due to the NSM-  
13 FRP bars. After debonding of the NSM-FRP bar, the load dropped suddenly and followed  
14 the curve of the corresponding control beam.

15 In terms of strains, the maximum NSM-FRP tensile strains at midspan for the tested  
16 beams are shown in Fig. 4. Composite action was achieved between the NSM-FRP and  
17 the concrete up to failure. This was indicated by the increase in the FRP tensile strain  
18 with the increase in load up to failure. The maximum measured NSM-FRP tensile strains  
19 for carbon and glass FRP bars were 75 and 85% of the ultimate FRP tensile strain,  
20 respectively.

#### 21 **Series A**

22 The control beam, A0, failed at load of 55.0 kN. While, beams AC1, AC2, AC3 and  
23 AC4 failed at loads of 67, 74, 94 and 96 kN with an increase in the ultimate load of about

1 22, 33, 71 and 75%, respectively. Thus, increasing the bonded length from  $24d$  to  $48d$   
2 increased the ultimate capacity by 29%. While, increasing the bonded length from  $48d$  to  
3  $60d$  increased the ultimate capacity by only 3%. This indicates that increasing the  
4 bonded length increases the ultimate load up to a certain limit beyond this limit any  
5 increase in the bonded length provide a small or no increase in the carrying capacity.

6

7 For beams AC5, AC6 and AC7, the size of the square groove was reduced to  $1.5d$  and the  
8 obtained ultimate load was 88, 94 and 102 kN, respectively. These ultimate loads are  
9 higher than their counterparts, AC2, AC3 and AC4, with groove size of  $2d$  by 19, 0, and  
10 6%, respectively. This indicates that the smaller groove size has insignificant effect on  
11 the strength for bonded length greater than  $24d$ .

12

13 Beams AC8 and AC9, strengthened with larger diameter (12.7 mm) CFRP bars and  
14 having bonded lengths of  $24d$  and  $48d$ , failed at loads of 74 and 109 kN, respectively.  
15 Thus, compared to beams AC2 and AC3, increasing the NSM-CFRP bar area by 79%  
16 increased the capacity by 1 and 16 % for beams AC8 and AC9, respectively. This  
17 indicates that the carrying capacity of the strengthened beams depends greatly on the  
18 bonded length.

19

20 Beams AG10 and AG11, strengthened with 12.7-mm diameter glass FRP bars and having  
21 bonded lengths of  $24d$  and  $48d$ , failed at loads of 75 and 112 kN, respectively. Compared  
22 to their counterparts with NSM-CFRP bars, AC8 and AC9, these failure loads provided  
23 an insignificant increase in the carrying capacity corresponding to 1 and 3%, respectively.

1 However, due to the low modulus of elasticity of the GFRP bars, beams strengthened  
2 with GFRP bars showed more deflection at failure (more than 2.5 times), and  
3 consequently higher ductility, than those utilizing CFRP bars (Table 3). This result makes  
4 it very attractive to further investigate the use of glass FRP bars in this technique.

5

### 6 **Series B**

7 The control specimen, B0, failed by steel yielding followed by concrete crushing at a load  
8 of 130 kN as shown in Fig.3. Beams BC1 and BC2 with a bonded length of  $24d$  and  $48d$ ,  
9 respectively, failed by debonding in a similar way to beams of Series A. The two beams  
10 showed 4 and 19% increase in the carrying load capacity. This indicates that the bonded  
11 length of  $24d$  was insufficient to develop the required strength in the NSM-FRP bars.  
12 Also, similar to beams of Series A, there was a decrease in the deflection at both yielding  
13 (10 to 20%) and failure (50 to 66%) load levels for both BC1 and BC2.

14

### 15 **Series C**

16 For the control beam C0, the yielding and failure loads were 204 and 233 kN,  
17 respectively, as shown in Fig. 3. Only 14% increase in the post-yielding strength (the  
18 difference between ultimate and yielding loads,  $P_{u,c} - P_{y,c}$ ) was observed.

19

20 Beams CC1, CC2, CC3, and CC4 showed small increase in carrying capacity ranged  
21 between 1 and 9%. The maximum increase in the carrying capacity, 9%, was attained by  
22 beam CC4 with the maximum tested bonded length of  $48d$ . This small increase in  
23 capacity can be explained as follows. Since NSM-FRP bar, with the relatively low

1 modulus of elasticity, is located farther from the neutral axis in comparison to steel bars,  
2 it is not expected to carry much load before steel yielding. Therefore, the lower the value  
3 between yielding of steel reinforcement and failure by debonding of the NSM-FRP bar,  
4 the lower the capacity enhancement achieved by the NSM-FRP system. Considering that  
5 the mode of failure for all strengthened beams was by debonding/splitting of concrete  
6 cover at the level of steel reinforcement, which occurred at the same state of stresses.  
7 Therefore, increasing the steel reinforcement ratio increases the yielding load and then  
8 reduces the range for which the NSM-FRP is active. Compared to other series, the  
9 percentage of steel reinforcement in Series C was the highest (1.60%) showing the lowest  
10 percentage of increase in capacity.

11

12 Although there was insignificant increase in the ultimate load; there was a decrease in the  
13 deflection at both yielding (8 to 12%) and failure (11 to 16%) load levels. This indicated  
14 that strengthening a beam increases its stiffness even if there is no increase in its ultimate  
15 capacity.

16

## 17 **NONLINEAR FINITE ELEMENT ANALYSIS**

18 A displacement-controlled nonlinear load–deformation analysis of FRP-strengthened  
19 concrete beams was carried out using the finite element package ADINA (Automatic  
20 **D**ynamic **I**ncremental **N**onlinear **A**nalysis) version 8.4 software (ADINA 2004). The  
21 formulations for the concrete, steel, and FRP of this software package are briefly  
22 summarized below.

23

## 1 **Geometrical Modelling**

2 Due to symmetry along two axes, only one quarter of the beam is modelled. Figure 5  
3 depicts a typical 3D mesh and the type of elements used. Eight-node brick elements are  
4 used to model the concrete, CFRP and epoxy layers. The steel reinforcement is simulated  
5 using 2-node truss elements. Three translational degrees of freedom are considered at  
6 each node. The interface elements between the epoxy and concrete nodes are aligned in  
7 the longitudinal direction of the beam (Detail B in Fig. 5), while, a full strain  
8 compatibility is assumed in the other two directions and also between the epoxy and FRP  
9 elements. Utilizing 3D modelling is proposed primarily to simulate the propagation of the  
10 cracks through the beam cross section.

11

## 12 **Material Models for Concrete, Epoxy, Steel and FRP**

13 A hypo-elastic model is utilized to describe the nonlinear stress–strain relationship for  
14 concrete as shown in Fig.6. The general multi-axial stress–strain relations are derived  
15 from the nonlinear uni-axial stress–strain relation shown in Fig.7a. Figure 7b depicts the  
16 concrete biaxial failure envelope. The ultimate uni-axial compressive stress,  $\sigma_u$ , is taken  
17 as  $0.85 f'_c$  and the ultimate uni-axial compressive strain,  $\varepsilon_u$ , is assumed to be 0.0035.

18 Also, Poisson's ratio,  $\nu$ , is taken as 0.18 for the concrete.

19 The behaviour of the cracked concrete is described assuming a system of orthogonal  
20 cracks. Once a crack occurs in any direction,  $i$ , the material is considered orthotropic with  
21 the directions of orthotropy being defined by the principal stress directions. Cracking of  
22 the concrete occurs when the principal tensile stress lies outside the tensile failure  
23 envelope.

1 The steel reinforcement is modelled as a bi-linear elastic-plastic material, with the  
2 tangent modulus in the strain-hardening regime taken to be one-hundredth of the elastic  
3 modulus. Also, a linear-elastic relationship until rupture is assumed for the FRP bars in  
4 which the elastic modulus in the direction perpendicular to the fibres,  $E_t$ , is assumed to  
5 be one-tenth of that in the direction of the fibres,  $E_f$ . This assumption has been  
6 generalized for 3D analysis since the experimental data do not address clearly the exact  
7 value of the transversal elastic modulus. The actual tensile strength, modulus of elasticity  
8 and strain at rupture of the FRP bars are used (Table 1). Furthermore, a linear-elastic  
9 model is employed to represent the mechanical characteristics of the adhesive layer. The  
10 Young's modulus is taken as 1500 MPa with a Poisson's ratio of 0.3.

11

#### 12 **FRP/Concrete Interface Models**

13 The interface elements are assumed between the epoxy and concrete nodes assuming a  
14 full bond between the FRP and epoxy nodes. This is done since the observed failure  
15 mode of the tested specimens was a separation of the concrete cover along the  
16 concrete/epoxy interface as shown in Fig. 7. Furthermore, no relative slips were observed  
17 between the NSM-FRP bars and the epoxy in the aforementioned experimental program.  
18 This leads to no further attention to the slip between the FRP bars and epoxy. However,  
19 the proposed interfacial model was meant for the interfacial behaviour of the layer  
20 beneath the longitudinal steel bars including the epoxy/concrete and epoxy/ FRP bars  
21 interfaces. The bond-slip relationships were driven from the experimental results of  
22 pullout tests of NSM-FRP embedded in concrete blocks (Soliman et al. 2007).

1 In this study, a full bond was assumed between the adhesive and the FRP reinforcement,  
2 for simplicity. The proposed bond-slip interfacial model (Soliman et al. 2007) is  
3 employed to represent the bond between the concrete and the adhesive. The bond-slip  
4 relationship correlates the local shear stress,  $\tau$ , and the associated slip,  $S$ , between the  
5 FRP bar and the concrete substrate.

6

## 7 **Finite Element Results and Discussion**

8 In the following section, a validation for the proposed model is made by a comparison  
9 between the experimental and the numerical results for test series A and B. Following  
10 validation of the proposed model, a parametric study is conducted to study a variety of  
11 factors that are known to affect the behaviour of strengthened beams. These factors  
12 include internal steel reinforcement ratio, concrete compressive strength, bonded length  
13 and area and the Young's modulus of NSM-FRP bars. The output responses of interest  
14 are the load-deflection profile, ultimate load carrying capacity and debonding strain in  
15 NSM-FRP bars.

16

### 17 **Validation of the proposed finite element model**

18 The numerical output is compared to the experimental results for selected beams from  
19 Series A and B. Table 4 summarizes the predicted and experimental load capacities,  
20  $P_{num.}$  and  $P_{exp.}$ , and the corresponding deflections at ultimate loads for the selected beams.

21 The comparison shows very good agreement between the numerical and experimental  
22 results. The average numerical-to-experimental load capacity ratio and its standard  
23 deviation are 1.05 and 0.023, respectively. Figures 8 and 9 show the load-deflection

1 relationships for series A and B, respectively. Figure 10 shows the predicted load-strain  
2 relationship for beams AC3 and AC4. It can be noticed from the curve that the debonding  
3 strain for the numerical analysis is slightly higher than the experimental one. This is due  
4 to the full bond assumption between the adhesive and the FRP, however, the difference  
5 could be accepted as it is less than 5%.

6

## 7 **Parametric study**

### 8 **Effect of the steel reinforcement ratio**

9 It has been demonstrated through the experimental program that the steel reinforcement  
10 ratio is one of the main factors controlling the efficiency of the NSM- FRP system. In this  
11 study, the effect of different steel reinforcement ratios on the predicted debonding load is  
12 investigated. The used steel reinforcement ratio varied between  $\rho_{s,min} = 0.2\sqrt{f'_c} / f_y =$   
13 0.2%, and  $\rho_{s,max} = 0.75\rho_{bal} = 3.0\%$ , where  $\rho_{min}$  and  $\rho_{bal}$  are the minimum and the balanced  
14 steel reinforcement ratio according to CSA/A23.3-04 (CSA 2004). Figure 11 shows the  
15 numerically predicted load-strain relationships for six beams having different steel  
16 reinforcement ratios of 0.2, 0.32, 0.76, 1.0, 2.0 and 3.0%. The six beams have the same  
17 strengthening scheme of one 9.5-mm diameter ( $71 \text{ mm}^2$ ) NSM-CFRP bar with a bonded  
18 length of  $48d$  in  $2d$  square groove. The mode of failure for the modelled beams is  
19 debonding of NSM-FRP bars from the surrounding concrete. This is simulated  
20 numerically when an interface element reaches  $\tau_{max}$  at a certain time step. In the  
21 subsequent time step, the slip value in this particular interface element tends to a huge  
22 value as a result of increasing the crack width passing through this element. Accordingly,  
23 the debonding numerically occurs at this particular element. From Fig. 11, it is obvious

1 that increasing the steel reinforcement ratio decreasing the beam ductility represented by  
2 the measured strains between yielding load and debonding failure load. Therefore, it can  
3 be stated that the efficiency of the NSM-FRP system is higher for beams with low steel  
4 reinforcement ratios compared to those with higher ratios. The effect of steel  
5 reinforcement has not been considered in any guidelines.

6

### 7 **Effect of concrete compressive strength**

8 Different concrete compressive strengths were used namely, 20, 30, 40 and 50 MPa. The  
9 four beams have the same strengthening scheme of one 9.5-mm diameter ( $71 \text{ mm}^2$ )  
10 NSM-CFRP bar with a bonded length of  $48d$  in  $2.0d$  square groove. As shown in Fig. 12,  
11 it can be concluded that generally increasing the concrete compressive strength increases  
12 both the debonding load and debonding strain level in the NSM-FRP bars. For concrete  
13 compressive strength of 20 MPa, no increase in the capacity was observed. When the  
14 compressive strength was increased to 30 MPa, approximately 10% increase in the  
15 capacity was achieved. This increase in the capacity was increased to 16% when the  
16 compressive strength was increased to 40 MPa. However, when the compressive strength  
17 was increased to 50 MPa, the increase in the capacity was only 17%. This indicates that  
18 the efficiency of using NSM-FRP is higher for stronger concrete up to a certain limit,  
19 after which no increase in capacity will be achieved.

20 Furthermore, the higher the concrete compressive strength, the smaller the crack width as  
21 well as the smaller the associated NSM-FRP bar slip values along the interface. In turn,  
22 the debonding strain increases. With the increase in the concrete compressive strength,

1 both the initial stiffness and cracking load increase as well yielding and debonding load  
2 levels.

3 As shown in Fig. 12, the debonding strain increases nonlinearly with the increase of the  
4 concrete compressive strength. This relationship has a similar trend to the one adopted by  
5 the ACI-440.2R-08 (ACI Committee 440 2008) for the debonding strain,  $\varepsilon_{fd}$ , in external  
6 strengthening

7 [1] 
$$\varepsilon_{fd} = 0.41 \sqrt{\frac{f'_c}{n.E_f.t_f}} \leq 0.9\varepsilon_{fu} \quad (\text{SI units})$$

8 where  $n$  is the number of FRP layers,  $E_f$  is the modulus of elasticity of the FRP,  $t_f$  is the  
9 thickness of an FRP layer, and  $\varepsilon_{fu}$  is the ultimate strain in the FRP. When using NSM bar,  
10 the value of  $n.t_f$  can be represented by  $A_f$ . However, there is no available formula in the  
11 codes and design guidelines for the debonding strain of NSM strengthening.

12 In the ACI-440.2R-08 design equation (ACI Committee 440 2008), the debonding strain  
13 increases in proportion to the square root of the concrete compressive strength. Similarly,  
14 equation (2) is employed in the *Fédération internationale du béton (fib 2001)* code. The  
15 formula considers only the concrete tensile strength and the axial stiffness of the FRP as  
16 parameters affecting the debonding strain,  $\varepsilon_{fd}$ . This design equation is given by:

17 [2] 
$$\varepsilon_{fd} = \alpha c_1 k_c k_b \sqrt{\frac{f'_c}{n.E_f.t_f}}$$

18 where  $\alpha$ ,  $k_c$ , and  $k_b$  are factors accounting for the influence of cracks on the bond  
19 strength, the state of compaction of the concrete, and the width factor, respectively. Also,  
20  $c_1$  is a factor determined experimentally.

21 The relationship between the debonding strain and the concrete compressive strength in  
22 these design guidelines and codes is approximately the same as presented in Fig. 12.

1 However, unlike the ACI and *fib* equations, the relationship between the debonding strain  
2 and concrete compressive strength stays constant after a strength value of 40 MPa.  
3 Although the predicted debonding strain is constant for concrete compressive strength  
4 greater than 40 MPa, the debonding load increases with the increase of the concrete  
5 compressive strength beyond this value (40 MPa) as observed in Fig. 12. This indicates  
6 that the increase in the ultimate capacity is attributed to the increase in the concrete  
7 strength rather than the FRP strain.

8

### 9 **Effect of axial stiffness (EA) of NSM-FRP bars**

10 The effect of the axial stiffness of the NSM-FRP on the debonding load and debonding  
11 strain levels is shown in Fig.13. As the axial stiffness (EA) of the NSM-FRP  
12 reinforcement increases the failure load increases and the debonding strain decreases.  
13 Therefore, increasing either the area of the NSM-FRP reinforcement (assuming enough  
14 concrete cover) or the modulus of elasticity of the NSM-FRP the effectiveness of the  
15 strengthening will be increased. This observation is in agreement with the ACI-440.2R-  
16 08 design equation (Eq. 1 above). The debonding strain reduces with the square root of  
17 the NSM-FRP axial stiffness. In terms of the load-deflection and load-strain  
18 relationships, the general trend of the profile does not depend on the axial stiffness value;  
19 however, the curve becomes steeper passing the yielding point.

20

### 21 **CONCLUSIONS**

22 Based on the experimental results, the following conclusions can be drawn:

- 1 • The mode of failure for the strengthened beams was debonding in the form of  
2 concrete cover splitting at the level of the internal steel reinforcement.
- 3 • The proposed NSM system, FRP bars and epoxy adhesive, is effective to increase  
4 both stiffness and flexural capacity of concrete beams. Compared to the  
5 unstrengthened beam, using NSM-FRP bars, with a bonded length of  $48d$ , increased  
6 the ultimate load of the tested beams by 9, 18, and 71% for beams with steel  
7 reinforcement ratios of 1.60, 0.80, and 0.40%, respectively. This means that the  
8 NSM-FRP system is more efficient when used with RC beams originally having  
9 low steel reinforcement ratio (in the range of  $\rho_{\min}$  to  $0.4\rho_{\text{bal}}$ ).
- 10 • Increasing the bonded length increases the ultimate carrying capacity up to a certain  
11 limit beyond which the increase in the bonded length will not result in any increase  
12 in the capacity. This limit is in the range of 48 times the bar diameter.
- 13 • Using a small groove size increases the distance between the FRP-NSM bar and the  
14 original steel reinforcement, which delays the concrete cover splitting and  
15 consequently higher capacities can be achieved.
- 16 • Compared to carbon FRP bars, GFRP bars as strengthening reinforcement provided  
17 nearly similar increases in the beam carrying capacity. However, due to the low  
18 modulus of elasticity of the GFRP bars, beams strengthened with GFRP bars  
19 showed more deflection at failure, and consequently higher ductility  
20 (deformability), than those utilizing CFRP bars. This result makes it very attractive  
21 to further investigate the use of glass FRP bars in this technique.

- 1 • The maximum measured NSM-FRP strains at failure was about 75 and 85% of the  
2 rupture strains of the FRP material for beams strengthened with CFRP and GFRP  
3 bars, respectively. This percentage depends on the bonded length of the FRP bar as  
4 the maximum NSM-FRP strains occurred for beams strengthened with bonded  
5 length of  $48d$  or greater.

6 Based on the results of the numerical analysis and parametric study, the following  
7 conclusions can be drawn:

- 8 • Previous investigations on strengthening using the NSM technique was assuming  
9 full bond between concrete, epoxy adhesive and NSM-FRP reinforcement.  
10 Apparently, this is the first analytical study on strengthening with NSM-FRP that  
11 takes into account the slip behaviour between FRP and concrete.
- 12 • The proposed finite element model was capable of accurately predicting the load-  
13 deflection behaviour and mode of failure of the strengthened beams with bonded  
14 lengths greater than  $24d$ . However, it was unable to predict the load-deflection  
15 behaviour for beams having a small bonded length. This was mainly due to the  
16 rapid premature failure of such beams.
- 17 • It was observed that increasing the steel reinforcement ratio increases the ultimate  
18 capacity of the RC strengthened beam. However, this is associated with reducing  
19 the debonding strain level in the FRP bars. This implicitly means that a higher  
20 efficiency of the NSM-FRP bars is obtained for beams with lower steel  
21 reinforcement ratios. This is in full agreement with experimental results.

- 1 • Increasing the concrete compressive strength increases both the debonding load and  
2 debonding strain level in the NSM-FRP bars.
- 3 • Increasing the axial stiffness for the NSM-FRP reinforcement increase the failure  
4 load and decrease the debonding the strain.

5

## 6 **ACKNOWLEDGEMENT**

7 The authors would like to express their special thanks and gratitude to the Natural  
8 Science and Engineering Research Council of Canada (NSERC), FQRNT (Subvention  
9 Équipe de recherche), ISIS Canada, Pultrall Inc. (Thetford Mines, Québec), Hilti Inc.  
10 (Montréal, Québec), and the technical staff of the structural laboratory in the Department  
11 of Civil Engineering at the University of Sherbrooke.

12

## 13 **REFERENCES**

14 ACI Committee 440 2004. Guide Test Methods for Fiber-Reinforced Polymers (FRPs)  
15 for Reinforcing or Strengthening Concrete Structures. ACI 440.3R-04, American  
16 Concrete Institute, Farmington Hills Michigan.

17 ACI Committee 440, 2002. Guide for the Design and Construction of Externally Bonded  
18 FRP Systems for Strengthening Concrete Structures. ACI 440.2R-02, American Concrete  
19 Institute, Farmington Hills Michigan.

20 ADINA. 2004. Automatic dynamic incremental nonlinear analysis: Finite element  
21 software version 8.2. ADINA R&D, Inc., Watertown, MA, USA.

1 Asplund, S. 1949. Strengthening Bridge Slabs with Grouted Reinforcement, ACI  
2 Structural Journal, American Concrete Institute, **20**(6): 397-406.

3 Benmokrane, B., El-Salakawy, E.F., El-Ragaby, A. and Lackey, T. 2006. Designing and  
4 testing of concrete bridge decks reinforced with glass FRP bars. ASCE, Journal of Bridge  
5 Engineering, **11**(2): 217–229.

6 Benmokrane, B., El-Salakawy, E., El-Gamal, S.E., and Sylvain, G. 2007. Construction  
7 and Testing of an Innovative Concrete Bridge Deck Totally Reinforced with Glass FRP  
8 Bars: Val-Alain Bridge on Highway 20 East. ASCE Journal of Bridge Engineering,  
9 **12**(5): 632-645.

10 Canadian Standard Association (CSA), 2004. Design of Concrete Structure for Buildings.  
11 CAN/CSA-A23.3 M-04, Canadian Standard Association, Rexdale, Ontario, Canada.

12 Canadian Standard Association (CSA), 2002. Design and Construction of Building  
13 Components with Fibre Reinforced Polymers. CAN/CSA-S806-02. Canadian Standard  
14 Association, Rexdale, Ontario.

15 Canadian Standard Association (CSA), (2006). Canadian High-Way Bridges Design  
16 Code. CAN/CSA-S6-06, Canadian Standard Association, Rexdale, Ontario.

17 Cruz JM S., Barros JAO. 2006. Bond between Near Surface Mounted Carbon Fiber  
18 Reinforced Polymer Laminate strips and Concrete. ASCE, Journal of Composites for  
19 Construction, **8**(6): 519-527.

20 De Lorenzis L. and Teng J.G. 2007. Near-Surface Mounted FRP Reinforcement: An  
21 Emerging Technique for Strengthening Structures. Composites, Part B: Engineering, 38:  
22 119–143.

1 El-Hacha, R. and Rizkalla, S. 2004. Near Surface Mounted Fiber Reinforced Polymer  
2 Reinforcements for Flexural Strengthening of Concrete Structures. ACI Structural  
3 Journal, American Concrete Institute, **101**(5): 717-716.

4 El-Salakawy, E.F. and Benmokrane, B. 2004. "Serviceability of Concrete Bridge deck  
5 Slabs Reinforced with FRP Composite Bars." ACI Structural Journal, Vol. 101, No.5, pp.  
6 727-736.

7 Hassan T. and Rizkalla S. 2004. Bond Mechanism of NSM FRP Bars for Flexural  
8 Strengthening of Concrete Structures. ACI Structural Journal, **101**(6): 830–839.

9 Hilti Inc. 2006. Product Technical Guide, <http://www.ca.hilti.com>.

10 Kang, J.Y., Park, Y.H., Park, J.S, You, Y.J. and Jung, W.T. 2005. Analytical Evaluation of  
11 RC Beams Strengthened with Near Surface Mounted CFRP Laminates, In Proceedings of  
12 the 7<sup>th</sup> International Symposium on Fibre-Reinforced Composite Reinforcement for  
13 Concrete Structures, (FRPRCS)-SP-230-45, volume 1, Shield C.K., Busel J., Walkup S.,  
14 Gremel D., editors, Michigan, USA, ACI, 779–794.

15 Kotynia, R. 2007. Analysis of the Flexural Response of NSM FRP-Strengthened  
16 Concrete Beams. In Proceedings of the 8<sup>th</sup> International Symposium of FRP  
17 Reinforcement for Concrete Structures, (FRPRCS-8), Fibre-Reinforced Polymer  
18 Reinforcement for Concrete Structures, Triantafillou T.C., editor.

19 Nanni, A., Ludovico, M. and Parretti R. 2004. Shear Strengthening of a PC Bridge Girder  
20 with NSM CFRP Rectangular Bars. Advances in Structural Engineering, **7**(4): 97-109.

21 Pultrall Inc. 2006. "Product Technical Specifications", <http://www.Pultrall.com>.

1 Soliman, S., M., El-Salakawy E. and Benmokrane B. 2007. Bond Properties of Near  
2 Surface Mounted (NSM) Carbon FRP Bars in Concrete. Proceedings on CD-ROM,  
3 Annual General Meeting & Conference Canadian Society of Civil Engineering, June 6-9,  
4 Yellowknife, Northwest Territories, Canada.

5 Soliman, S., M., El-Salakawy, E. and Benmokrane, B. 2008a. Flexural Behaviour of  
6 Concrete Beams Strengthened with Near Surface Mounted FRP Bars. Proceedings on  
7 CD-ROM, Fourth International Conference on FRP Composites in Civil Engineering  
8 (CICE2008), 22-24 July, Zurich, Switzerland.

9

1 Table 1 - Mechanical properties of the reinforcing bars

Bar type	Bar diameter mm	Bar area mm <sup>2</sup>	Modulus of elasticity, GPa	Tensile strength, MPa	Ultimate strain %
CFRP	9.5	71	124±5	1596±31	1.40±0.00
	12.7	127	134±9	1250±50	0.74±0.05
GFRP	12.7	127	45±1	756±27	1.80±0.04
Steel*	11.3	100	200	$f_y = 454$ $f_u = 571$	$\epsilon_y = 0.21$
	15.9	200	200	$f_y = 460$	$\epsilon_y = 0.21$
				$f_u = 558$	

2 \* Steel properties are those reported by the manufacturer

3

4

5

6 Table 2 - Description of test specimens for the flexural strengthening:

Beam code	Type of FRP	Diameter of FRP (mm)	Groove dimension	Bonded length
Series A ( $\rho_{steel} = 0.4\%$ )				
A0	-----	-----	-----	-----
AC1	Carbon	9.5	2d	12d
AC2				24d
AC3				48d
AC4				60d
AC5	Carbon	9.5	1.5d	24d
AC6				48d
AC7				60d
AC8	Carbon	12.7	2d	24d
AC9				48d
AG10	Glass	12.7	2d	24d
AG11				48d
Series B ( $\rho_{steel} = 0.8\%$ )				
B0	-----	-----	-----	-----
BC1	Carbon	9.5	2d	24d
BC2				48d
Series C ( $\rho_{steel} = 1.6\%$ )				
C0	-----	-----	-----	-----
CC1	Carbon	9.5	2d	12d
CC2				18d
CC3				24d
CC4				48d

7 Note:  $d$  is the diameter of the NSM-FRP bar

8

9

1 Table 3 – Summary of test results for the tested beams

Specimens code	Bonded length $L_b$	Yield load $P_y$ , kN	Failure load $P_u$ , kN	Ultimate deflection $\Delta u$ , mm	Ductility index	NSM-FRP debonding strain, $\mu\epsilon$	Failure mode	Ultimate capacity increase %
A0	—	52	55	76	11.21	—	Y	—
AC1	12 <i>d</i>	58	67	17	2.04	2,423	Cs	22
AC2	24 <i>d</i>	54	73	25	3.58	5,058	Cs	33
AC3	48 <i>d</i>	58	94	24	3.25	8,583	Cs	71
AC4	60 <i>d</i>	60	96	27	2.96	8,595	Cs	75
AC5	24 <i>d</i>	65	88	31	2.97	6,464	Cs	60
AC6	48 <i>d</i>	72	94	25	2.00	9,012	Cs	71
AC7	60 <i>d</i>	61	102	37	3.28	12,400	Cs	85
AC8	24 <i>d</i>	59	74	20	2.56	2,026	Cs	34
AC9	48 <i>d</i>	76	109	19	1.91	5,650	Cs	98
AG10	24 <i>d</i>	54	75	26	3.00	7,515	Cs	36
AG11	48 <i>d</i>	59	112	49	5.56	15,333	Cs	104
B0	—	96	130	62	5.69	—	Y	—
BC1	24 <i>d</i>	114	135	21	1.62	6,252	Cs	4
BC2	48 <i>d</i>	115	154	31	2.78	10428	Cs	18
C0	—	204	233	27	1.95	—	Y	—
CC1	12 <i>d</i>	206	227	24	1.86	2,534	Cs	-3
CC2	18 <i>d</i>	213	229	23	1.59	3,270	Cs	-2
CC3	24 <i>d</i>	215	234	20	1.39	5,065	Cs	0
CC4	48 <i>d</i>	216	254	23	1.6	6,244	Cs	9

2 Note: *d* is the diameter of the NSM-FRP bar; Y: steel yielding Cs: concrete cover splitting

3

4 Table 4 - Comparison of experimental and numerical results for series A and B

specimen	Experimental		Numerical		$P_{num}/P_{exp}$
	Failure load, $P_{exp}$ , kN	Deflection, mm	Failure load, $P_{num}$ , kN	Deflection, mm	
AC3	94	24	96	24	1.03
AC4	96	27	103	27	1.06
B0	130	62	139	65	1.06
BC1	135	21	142	22	1.05
BC2	154	31	160	34	1.04
				average	1.05
				Stand. dev.	0.023
				C.O.V.	2.17

5

6

1

2 **List of Figures**

3 Fig. 1 - Dimensions and reinforcement details of test beams

4 Fig. 2 - Test setup

5 Fig. 3 - Load-deflection relationships

6 Fig. 4 - Load-strain relationships

7 Fig. 5 - Types of elements used for the strengthened beams

8 Fig. 6 - Constitutive laws of used materials: a. Concrete in uni-axial stress, b. Bi-axial

9 concrete failure envelope

10 Fig. 7 - Separation of the concrete cover along the concrete/epoxy interface

11 Fig. 8 - Comparison between numerical and experimental load-deflection relationships

12 for beams of Series A

13 Fig. 9 - Comparison between numerical and experimental load-deflection relationships

14 for beams of Series B

15 Fig. 10 – Strains in the NSM-FRP bar for beam AC3 and AC4

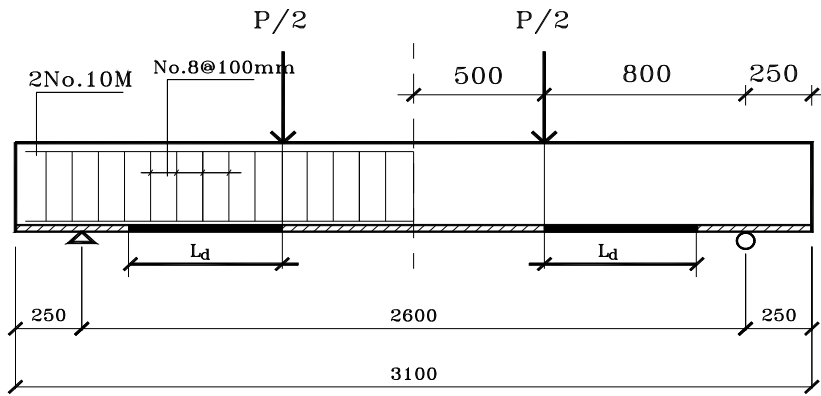
16 Fig. 11 - Effect of the steel reinforcement ratio on load–strain relationships

17 Fig. 12 - Effect of concrete compressive strength on failure load and FRP debonding

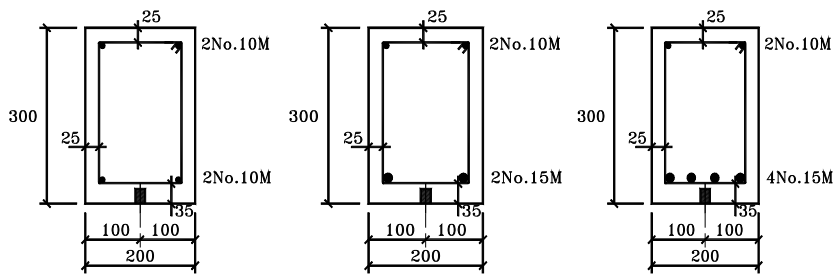
18 strain

19 Fig. 13 - Effect of axial stiffness on failure load and FRP debonding strain

20



1



2

3

Series A

Series B

Series C

4

5

6

7

8

9

10

11

12

13

14

15

1

2



3

4

5

6

7

8

9

10

11

12

13

14

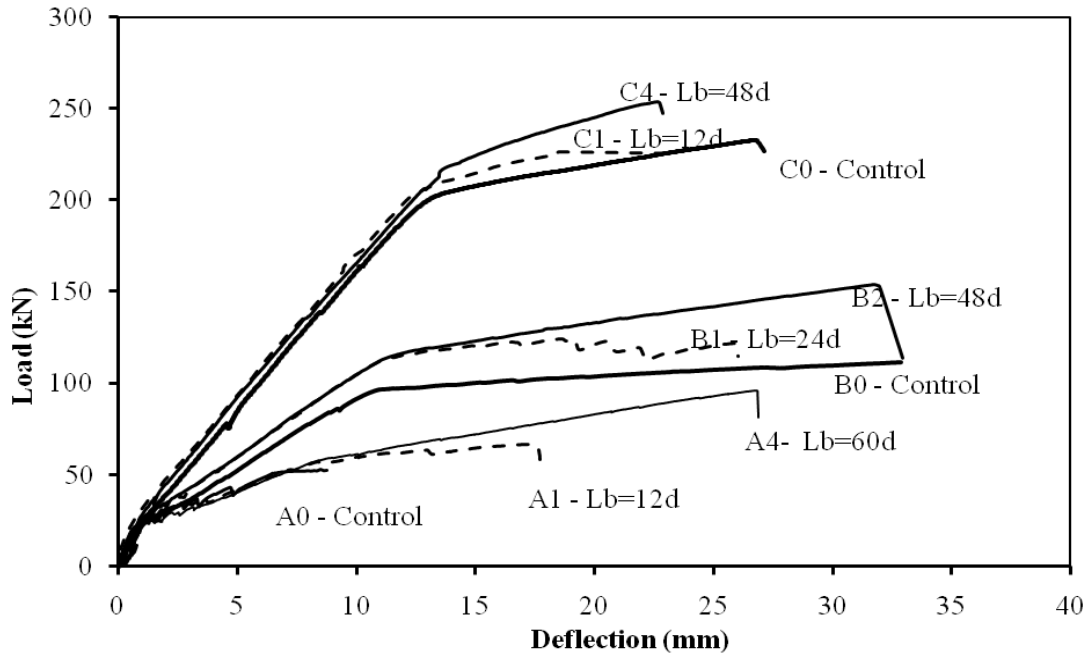
15

16

17

1

2



3

4

5

6

7

8

9

10

11

12

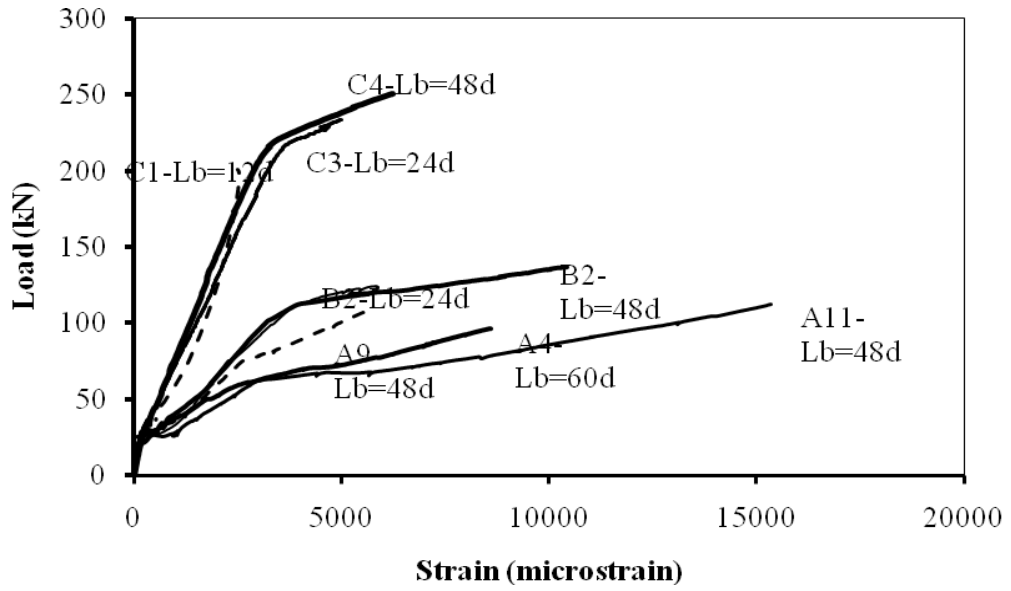
13

14

15

1

2



3

4

5

6

7

8

9

10

11

12

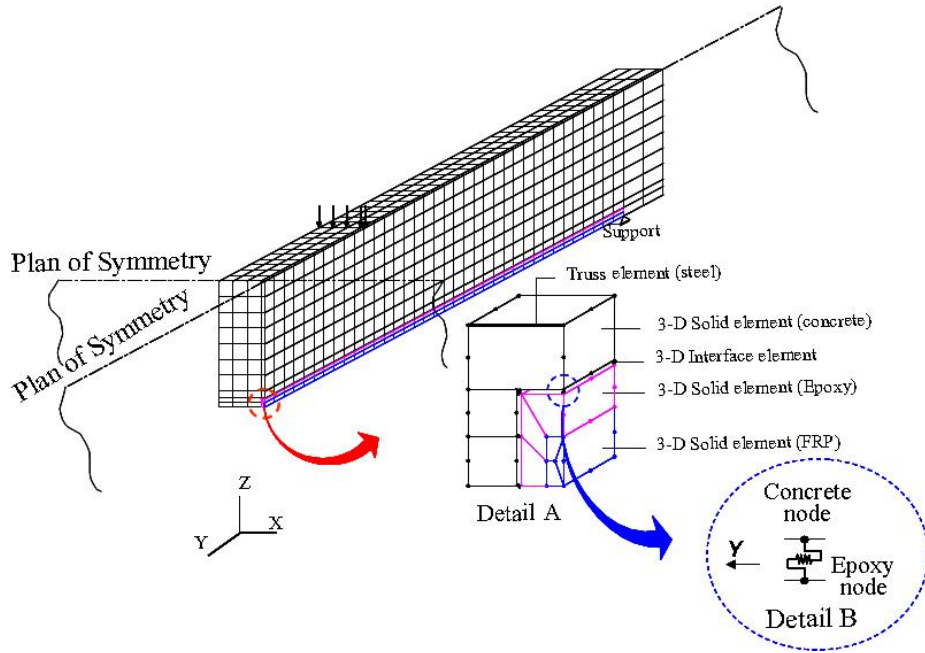
13

14

15

1

2



3

4

5

6

7

8

9

10

11

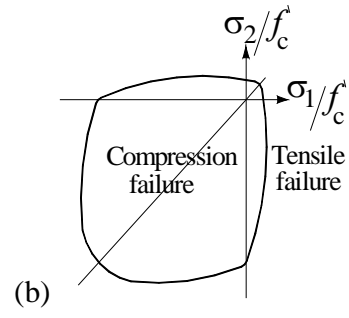
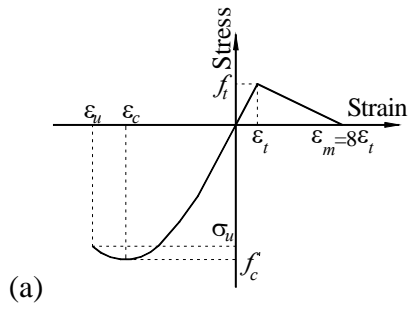
12

13

14

15

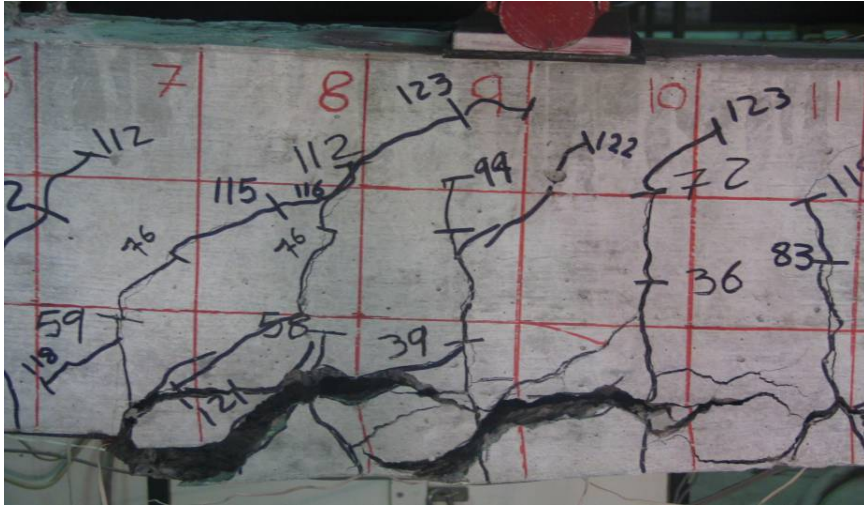
1  
2  
3  
4



5  
6  
7  
8  
9  
10  
11  
12  
13  
14  
15  
16  
17  
18  
19  
20

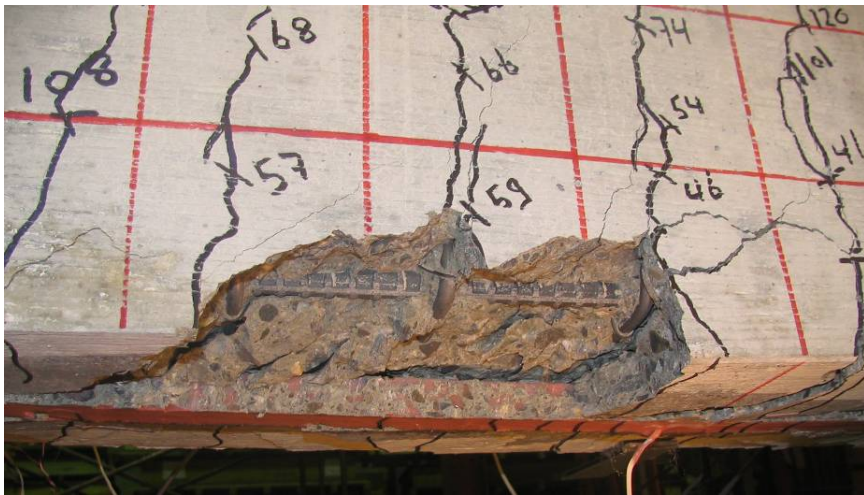
1

2



3

4



5

6

7

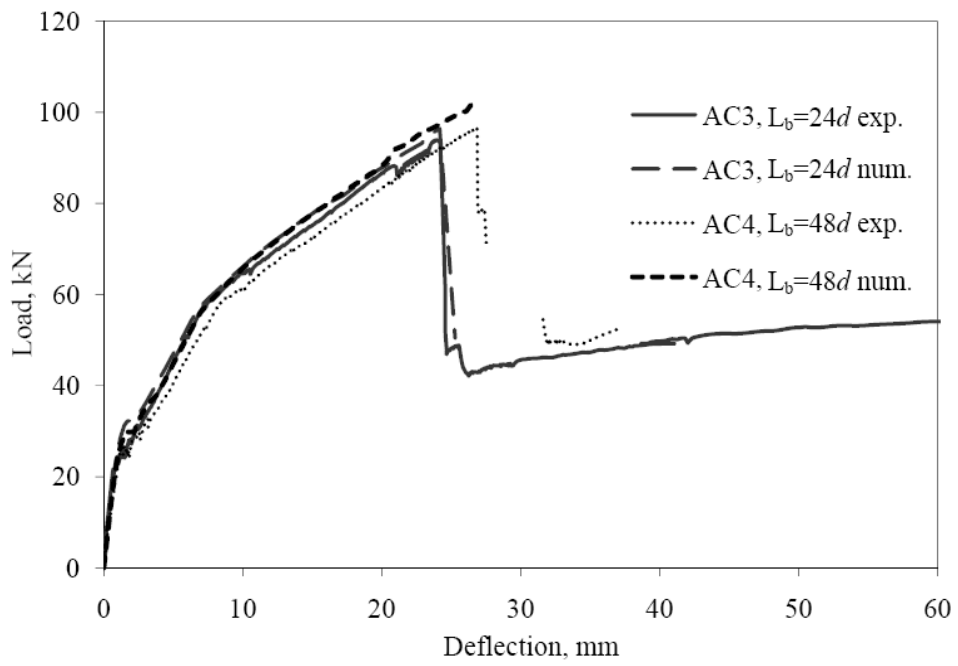
8

9

10

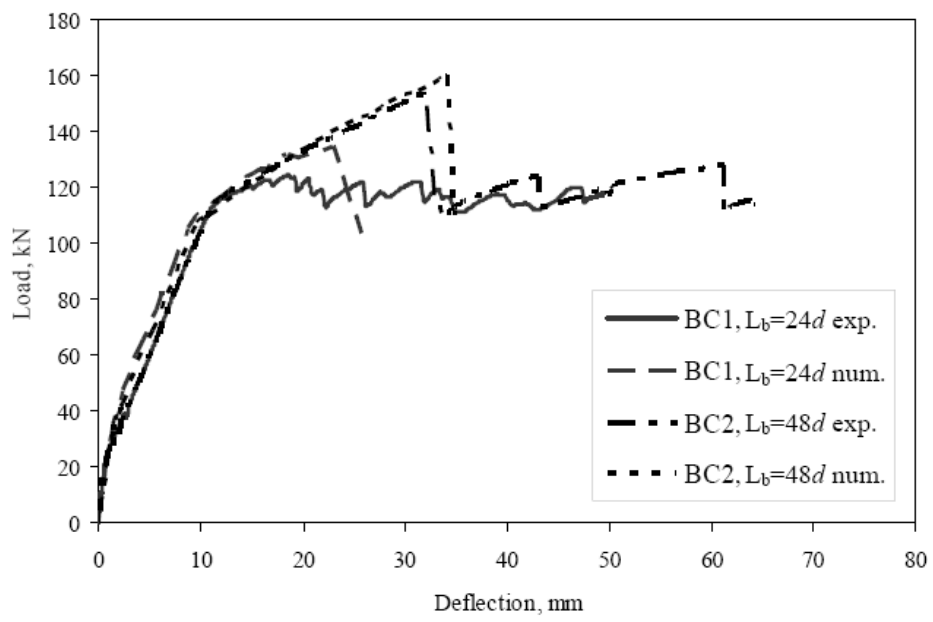
11

1  
2  
3  
4  
5  
6  
7



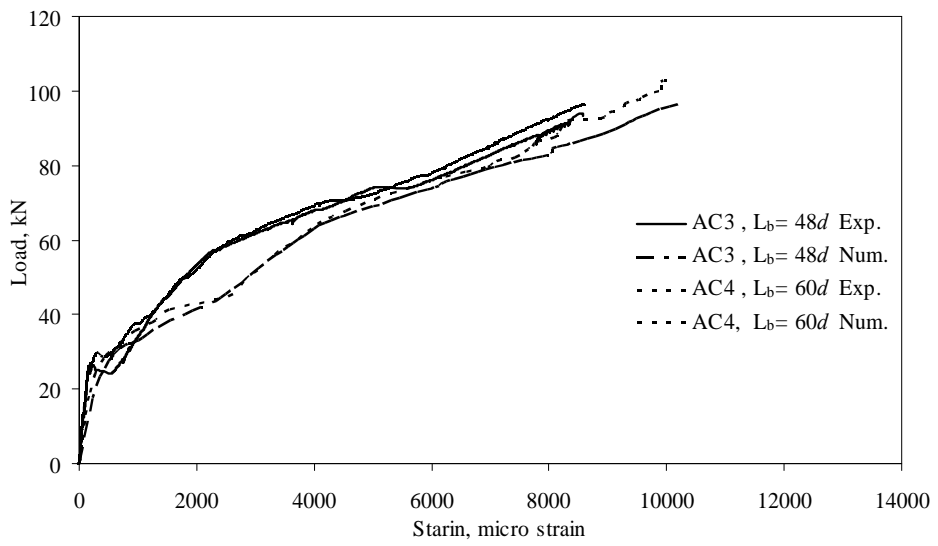
8  
9  
10  
11  
12  
13  
14

1  
2  
3  
4  
5  
6  
7  
8  
9



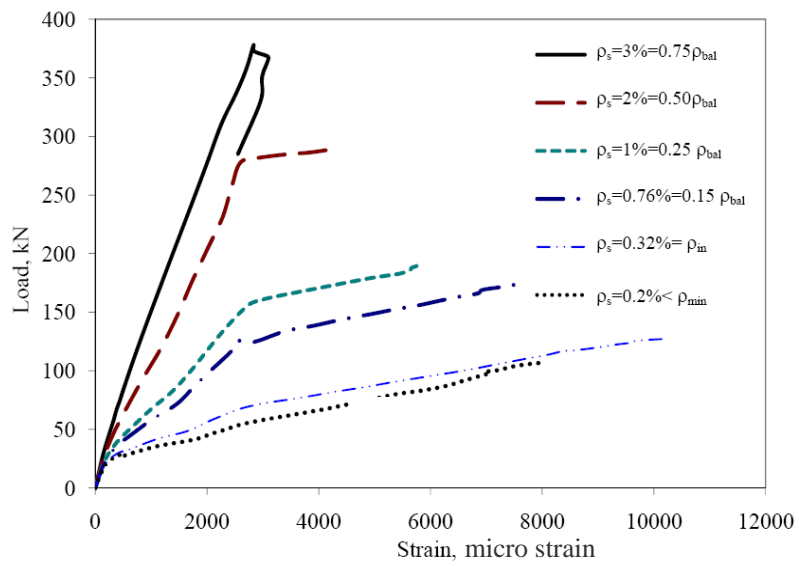
10  
11  
12  
13  
14  
15

1  
2  
3  
4  
5  
6  
7  
8  
9



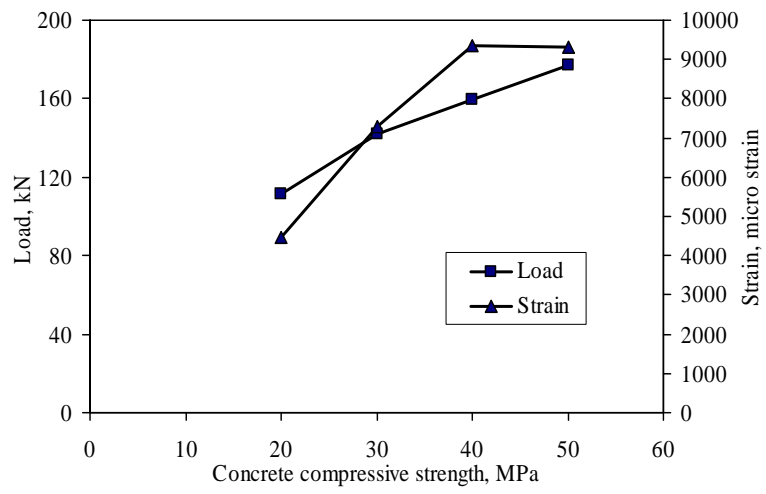
10  
11  
12  
13  
14  
15  
16

1  
2  
3  
4  
5  
6  
7  
8  
9



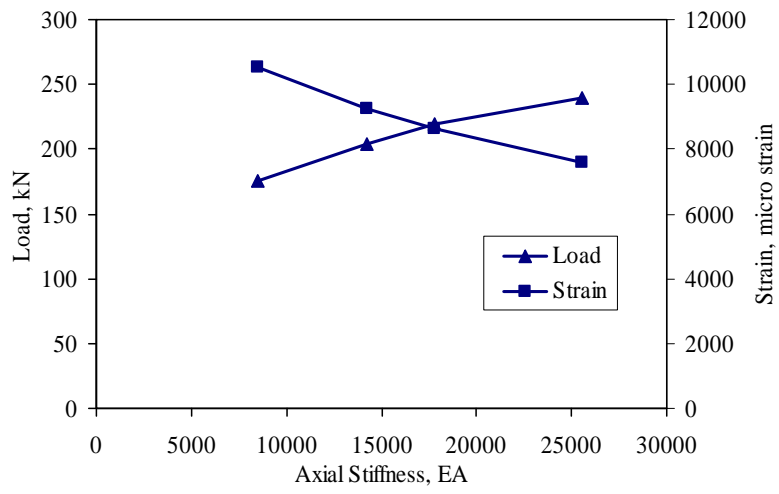
10  
11  
12  
13  
14  
15  
16

1  
2  
3  
4  
5  
6  
7  
8  
9



10  
11  
12  
13  
14  
15  
16  
17

1  
2  
3  
4  
5  
6  
7  
8  
9



10  
11  
12